STRUCTURE AND PROPERTIES OF STRONTIUM PHOSPHATE GLASSES MODIFIED WITH ALUMINUM OXIDE APPLIED AS GLASS IONOMER CEMENT

G. El-Damrawi[1], D. Shosha[1], A. M. Abdelghany[2,3] and M. I. Abdelghany[1,3*]

[1]Glass Research Group, Physics Department, Faculty of Science, Mansoura University, 35516, Mansoura, Egypt
[2]Spectroscopy Department, Physics Division, National Research Centre, 33Elbehouth St., Dokki, 12311, Giza, Egypt
[3]Basic Science Department, Horus University, International Coastal Road, New Damietta, Kafr Saad, Damietta, Egypt

ABSTRACT. Studied glasses in the system $50P_2O_5$-$(49-x)$SrO-$1AlF_3$-xAl_2O_3 (mol%), $0 \leq x \leq 4.5$, were prepared via the melt-annealing technique. The prepared samples are transparent amorphous network structures. Glasses are still transparent upon the heat treatment at 540 °C for 4 hours. ^{27}Al nuclear magnetic resonance (NMR) has been applied to determine the structural role of Al_2O_3. X-ray diffraction (XRD), Fourier transform infrared (FTIR), and Vickers hardness (H_v) measurements have been carried out. XRD spectroscopy is used to investigate the glasses' crystalline features. The crystallinity was enhanced via the heat treatment process. Some of investigated strontium phosphate glasses are recommended to be applied in dental applications.

KEY WORDS: NMR, Aluminum oxide, GIC, X-ray diffraction, Strontium phosphate

INTRODUCTION

In the last few decades, phosphate glasses have attracted much attention from many researchers due to their unique properties (compared to borate and silicate glasses). P_2O_5 glasses are characterized by their high thermal expansion coefficient, low glass transition temperature, viscosity, softening and melting temperatures, and high transmission in the UV region [1-3]. According to such properties, which led to significantly improved their use in a number of technological domains, such as the vitrification of some radioactive wastes [4], photonics [5], fast ion conductors, energy transfer materials [6], glass to metal seals [7], bio-medical engineering [8], and radiation therapy [9]. Phosphate glasses have low thermo-optical coefficient and high emission, so, they can be considered the suitable materials for high power laser materials. The range of applications of phosphate glasses can be enhanced by adding one or more intermediate oxides such as CaO, CuO, Al_2O_3, etc., which can improve its physical properties [10-12]. The addition of different cations to glass network increases its cross-link density (enhance chemical durability). Most recently, glasses or glass-ceramics containing Al_2O_3, such as Al_2O_3-B_2O_3, Al_2O_3-SiO_2, or Al_2O_3-B_2O_3-SiO_2, and Al_2O_3-P_2O_5 systems, have gotten a lot of attention [13-16]. Because of the existence Al_2O_3 can form interconnected bonds in glass systems, leading to an improvement in the chemical stability [17] and good mechanical properties [18, 19]. Physical properties of Al_2O_3-containing glasses, such as chemical durability, conductivity and micro-hardness, are strongly linked to their Al-coordination, The Al_2O_3 can enhance the toughness and hardness of the glass and makes the material durable against corrosion. In addition, Al_2O_3 oxide gives a significant advantage to the material by enhance the hardness and other mechanical properties to be used as compatible dental fillers [20-21].

---

*Corresponding author. E-mail: ph_abdelghany@mans.edu.eg

SrO-phosphate glasses [22], have been investigated via the analyses of FTIR spectroscopy. Such results show that strontium ions act primarily as glass modifiers. The number of non-bridging oxygen (NBO) per tetrahedron on average in the structure of strontium phosphate glasses increases with increasing SrO content. With increasing SrO content, the P=O bonding intensity in the phosphate glasses decreases; O-P-O bonding is diminishing, while P−O bond strength increases. Two main types of strontium sites-modifier and former are documented to be present [23].

The advantage of metal oxide glasses such as SrO is that they can be crystallized since, in comparison to glasses free of SrO, high crystallinity is achieved by lowering the sintering temperature. Strontium oxide can speed up the rate of reaction between the phosphate solution and tested sample. Glass ceramics containing SrO is highly active than that SrO-free phosphate glasses. Therefore, the presented work aims to shed light on the structural role played by Al_2O_3 and SrO in strontium phosphate glass and their role in the enhancement of glass ionomer cement (GIC) formation.

EXPERIMENTAL

Glass preparation

Strontium phosphate glasses samples were prepared via ordinary melt annealing technique. The glass samples from the system $50P_2O_5$-$(49-x)$SrO-$1AlF_3$-xAl_2O_3 (mol%) where $0 \leq x \leq 4.5$ were prepared using chemically pure raw materials as shown in Table 1. Ammonium phosphate monobasic ($NH_4 H_2PO_4$) (98%, Sigma Aldrich) is the source of P_2O_5, and $SrCO_3$ (99.9+%, Sigma Aldrich) is the SrO source. Using a micro-analytical balance, the specific amount of each raw material was weighed and mixed according to the molar composition ratio. The well-mixed composition was pre-heated at 300 ºC for 30 min. in a 50 mL porcelain crucible to remove unwanted components, such as NH_3 and H_2O, and then the electric furnace temperature is increased to 1150 ºC for 1 hour and homogenization was achieved by stirring for about 30 min onto warmed stainless-steel plates, the melted samples were poured with the required dimensions. The annealing process at 300 ºC/1 h was started immediately by transferring samples into a muffle furnace. Then, at a rate of 25 ºC/h, the samples were left to cool to room temperature.

Table 1. Glass compositions of prepared glasses.

Sample	SrO	P_2O_5	AlF_3	Al_2O_3
a	49	50	1	0
b	48	50	1	1
c	46.5	50	1	2.5
d	46	50	1	3
e	45.5	50	1	3.5
f	45	50	1	4
g	44.5	50	1	4.5

Measurements

Measurements of X-ray diffraction were carried out with a Shimadzu X-ray diffract meter (Model Dx-30, Egypt). The intensity and position of peaks of XRD patterns were compared with patterns in the international powder diffraction file (PDF) database compiled by the joint committee for powder diffraction standards (JCPDS). ^{27}Al NMR measurements were carried out at ambient temperature on a JEOLRESONANCE (GSX-500) spectrometer operating at a high external magnetic field (11.747 T). ^{27}Al NMR spectra were measured at the resonance frequency of 130.2 MHz, using a 3.2 mm MAS NMR probe operated at a rotor frequency of 15 kHz. Typical pulse

lengths were 2.5 μs and 60 s delay time was sufficient to enable relaxation. Spectra are referenced to $Al(NO_3)_3$ (0 ppm). ^{27}Al NMR spectra were fit with Delta NMR software, version 5.04 (Japan) has been used for NMR analysis (Faculty of Science, Mansoura University). The hardness of the specimens was determined using a digital Vickers microscope model (FM-7, Future-Tech Corporation, Kawasaki-Japan). The Vickers's hardness (H_v) test was performed under 50 g load and 15 s dwell time. The FTIR spectra for obtained samples were carried out utilizing the KBr pellets technique. The spectra are measured in the region of 400-4000 cm^{-1} with a spectral resolution of 2 cm using a Mattson (5000) FTIR spectrometer (Faculty of Science, Mansoura University).

RESULTS AND DISCUSSION

X-ray diffraction (XRD)

The X-ray diffraction patterns for the studied $1AlF_3$-xAl_2O_3-$(49-x)SrO$-$50P_2O_5$ (mol%) glasses with different additive concentrations from Al_2O_3 are shown in Figure 1. The spectra confirmed the amorphous behavior of all of the investigating samples. The amorphous phase profiles show no sharp peaks, just humps lie between $2\theta \sim 10–40$ at all concentrations.
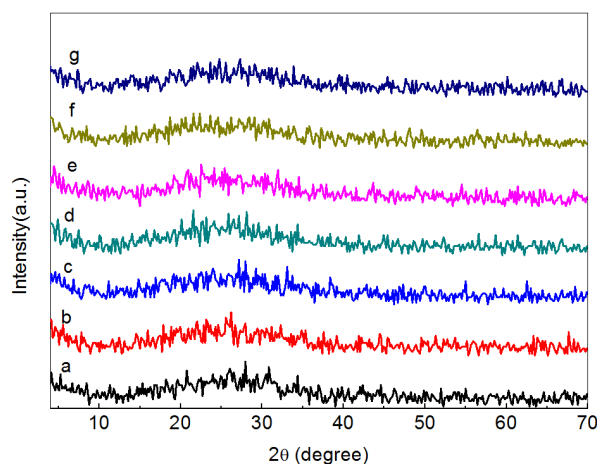

Figure 1. XRD patterns for the studied Al_2O_3-strontium phosphate glasses.

   In the field of application, the glasses should be thermally treated to contain some specific polycrystalline species which gives the material the advantage of biocompatibility and/or bioactivity. Therefore, the as-prepared glasses are treated thermally (or heat treatment (H.T.)) at about 540 °C for 4 hours to transform the amorphous glass to glass ceramics as shown in Figure 2.
   XRD pattern of the heat-treated samples is shown in Figure 2, the spectra contain some sharp diffraction peaks superimposed on a broad amorphous background. The intensity of the sharp diffraction lines is gradually increased with increasing Al_2O_3 content at expense of SrO which leads to an increase in the percentage of crystalline species to become maximum at an Al_2O_3 concentration of 3 mol% and then decreases. Then the sample containing 3 mol% Al_2O_3 is considered a suitable composition presenting transparent glass ceramic material after the thermal heat treatment process. From the XRD pattern and cards, Figure 2, it can be predicted that crystalline $Sr_3(PO_4)_2$ [JCPDS Card No.85-905] and $SrAl_3(PO_4)_3F_2$ phases [JCPDS Card No.87-874] are produced upon treating the glass thermally.
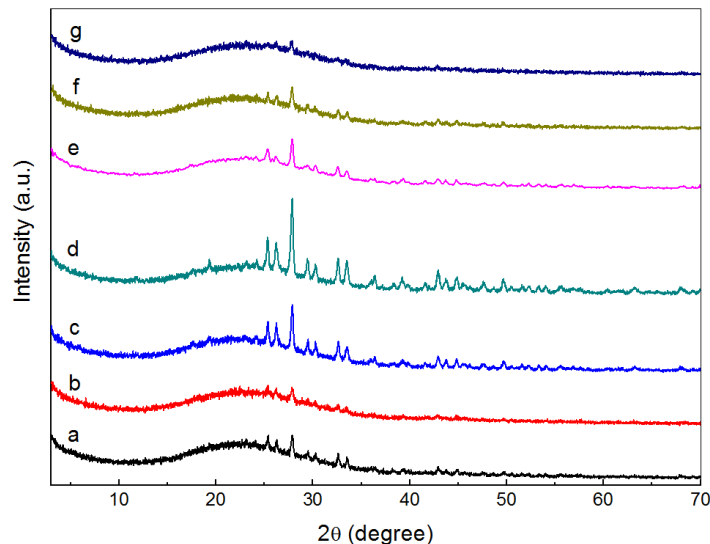
Figure 2. XRD patterns for Al_2O_3-strontium phosphate glasses after H.T. 540 °C/4 h.

Nuclear magnetic resonance (NMR)

Figure 3 represents ^{27}Al NMR spectra of one of the compositions of prepared Al_2O_3-strontium phosphate glasses. A high intense ^{27}Al NMR resonance of chemical shift at about 45 ppm arising from four-coordination Al(4) was seen for glasses containing 3 mol% Al_2O_3 presented as an example for all investigated compositions. This figure indicates that the main portion of the aluminum is principally acting as a network-former (AlO_4) species. Each added Al_2O_3 molecule is equivalent to a decrease of one SrO molecule. This leads that most of Al_2O_3 entering as a glass former. The broad spectral resonance band, figure 3, evidenced that no of Al_2O_3 enters as six-coordination Al(6) in the studied glasses. Similarly, there is no appearance of the five-coordination Al(5) within the glass. This shows that the excess of SrO-Al_2O_3 should associate itself with PO_4 tetrahedral forming AlO_4-PO_4 linkages. Figure 3, the resonance spectra were found to have contributed to the formation of the observed low peak which can represent Al_4-O-P at about 41 ppm. the NMR spectrum accurate integration gives more precise information concerning the relative amount of these structural elements was possible owing to the separation of the spectra into their component bands [24]. The analyzed broad peak around 46 ppm represents AlO_4 tetrahedral units. This species (AlO_4) is expected to be formed since the glasses are enriched with SrO as a modifier and there is no ability to Al_2O_3 to play the role of SrO as a modifier.

In this case, most of Al_2O_3 would suppress the continued formation of NBO in the phosphate network [25]. This is because Al_2O_3 enters as a glass former (AlO_4) which is compensated with some SrO as a modifier. Then increasing Al_2O_3 at expense of SrO can reduce NBO in the phosphate network due to building a stronger Al_4-O-P unit than that of weaker P-O⁻ Sr⁺ non-bridging bonds. Then one can confirm that SrO is a modifier, P_2O_5 is a strong glass former and Al_2O_3 can also play a role of a glass former.
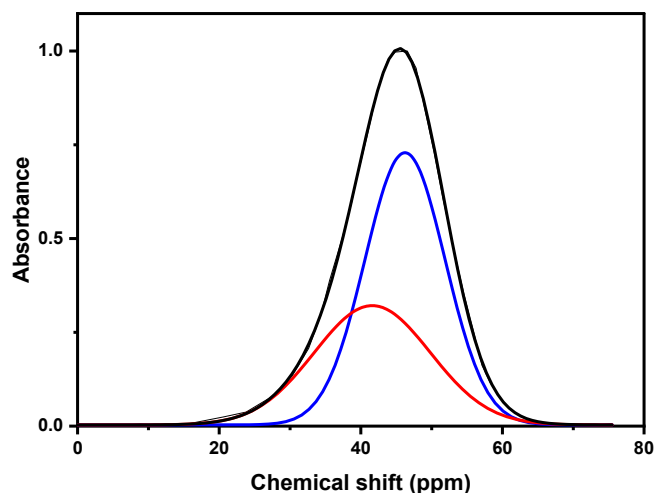
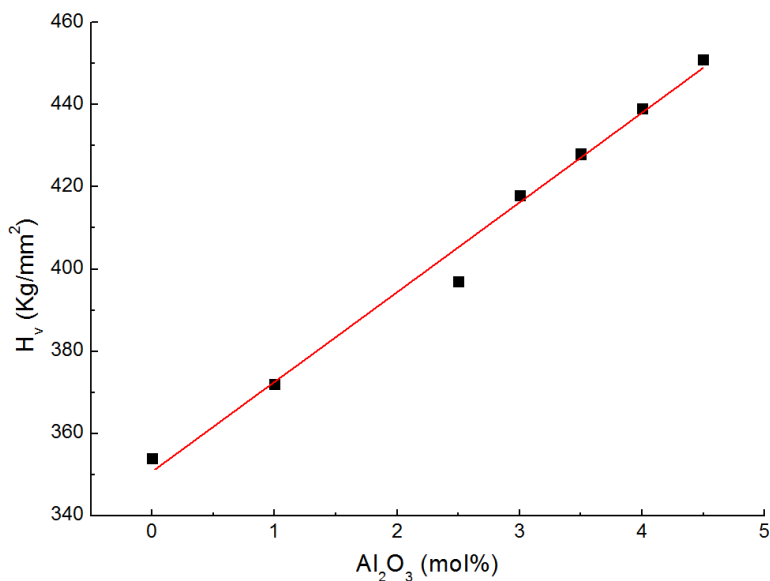Figure 3. ^{27}Al NMR spectra of strontium phosphate glass containing 3 Al_2O_3 mol%.

Figure 4. Hardness of Al_2O_3-strontium phosphate glass after H.T. at 540 ºC/4 h.

Microhardness measurements (Hv).

Increasing of Al-O-Al and Al-O-P bonds with increasing Al_2O_3 plays the role of enhancing the mechanical properties of the material. In this regard, increasing Al_2O_3 leads to increasing the hardness number of the investigating glasses (Figure 4). Concerning the hardness of the investigated samples, both the increase of the Al-O-P bonds in parallel with bridging oxygen

formation and free volume reduction leads to a hardness increase with increasing Al_2O_3 content. In addition, mixed-forming structural units containing bringing bonds which are formed at the expense of orthophosphate groups also have some effect. This is because the more formed P-O-P and Al-O-Al bonds and more compact structure can withstand the material against penetration and increases the hardness number. This consideration was agreed well with the quantitative analysis based on NMR data, which demonstrated the transformation of some NBO sites into bridging oxygen (BO) ones, confirming the presence of a more shielded phosphate network resulting in enhancing hardness number [26].

Infrared absorption spectra

FTIR spectra of Al_2O_3-free SrO-P_2O_5 glass and glass containing Al_2O_3 are shown in Figure 5. The glass is found to exhibit a wide absorbed hump that lies in the frequency range 800-1500 cm^{-1} [27, 28]. The relative area and intensity of this band become narrower and decreases with increasing Al_2O_3 contents. This behavior would be related to the formation of mixed P—O—Al and P—O—P bonds which have been evidenced by NMR spectra of aluminum-containing glass. Increasing Al_2O_3 at expense of SrO leads to increasing the covalence of Al_4—O—P at expense of the ionic bonded species (P—O—Sr^+). This may lead to an increasing number of bridging oxygen atoms between Al and P which in turn increase Q^2 at the expense of Q^1 and Q^o. In addition, Q^3_2 units should be increased. The latter means that most phosphate units contain 3 BO oxygen bonds, two of them are formed in the P—O—P shape and one is a P—O—Al bond. Decreasing in P-O-Sr bond and increase of Al—O—P ones is considered as the main reason for decreasing of FTIR band area of the studied glasses with increasing Al_2O_3 at the expense of SrO (Figure 5).
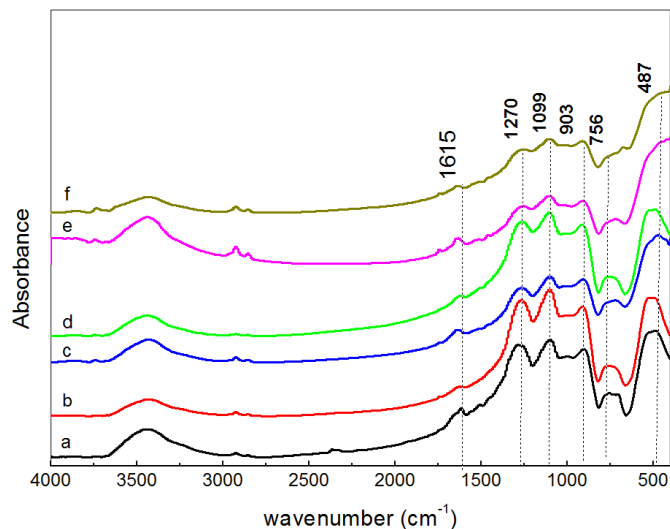

Figure 5. FTIR spectra of glasses of the basic constituents 50 P_2O_5-49 SrO-1 AlF_3 and doped with different concentrations of Al_2O_3.

Different absorption bands were observed in Figure 5, the band centered at 487 cm^{-1} is assigned to the bending vibrations of O—P—O units overlapped with metal cation vibration. The two absorption bands located at 756 and 903 cm^{-1} are attributed to the symmetric and asymmetric stretching vibrations respectively of P—O—P bonding [29, 30]. The band centered at around

1099 cm^{-1} is attributed to an asymmetric stretching vibration of P—O. The absorption band at 1283 cm^{-1} is assigned to the asymmetric stretching vibration mode of the O—P—O bonding, denoted by ν_{as} (PO$_2$). The absorption bands at 1615 cm^{-1} are due to the water, OH, and P—O—H vibrations. The effect of introducing Al$_2$O$_3$ in the glass's matrix produced limited changes as focused on loosely bonded groups and the reformation of some phosphate groups.

Figure 6 represent FTIR spectra for samples containing different concentration of Al$_2$O$_3$ and treated thermally. In comparison between Figures 5 and 6, it can be observed that some differences refer to the thermal heating process. Sharper FTIR bands are considered for glass treatment. The sharper bands may be considered to be due to the formation of even small-sized crystals in the main host glass network which was confirmed by the XRD patterns figure.
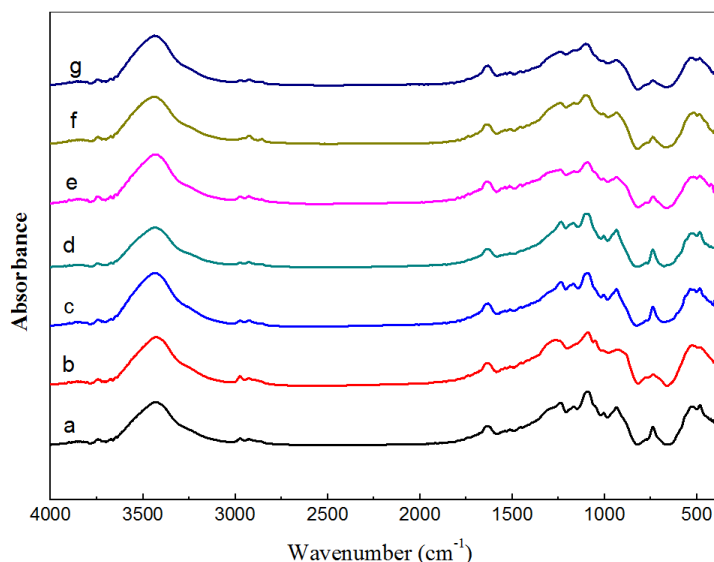

Figure 6. FTIR spectra of Al$_2$O$_3$-strontium phosphate glasses after H.T. 540 ºC/4 h.

The formation of crystalline structural species is considered a useful type required to construct GIC which is obtained as a result of the acid-base reaction between weak water acid usually poly acrylic acid and the powered sample of the crystalline glasses as shown in Figure 7.

According to the results obtained in Figure 7, there is an intensive FTIR absorbed band lies in the region 1600 to 1800 cm^{-1} represents the acid-base reaction, such band may represent C—O and Sr—O vibration in the strontium carboxyl groups which is called cement matrix [31, 32]. This intense band didn't appear in the spectra of both prepared or thermally treated glasses. These changes confirm that the acid-base reaction had been completely carried out. The acid attacks some elements found in the glass powder and as a result of the released Sr, CO$_2$ can interact with PO$_4$ units to yield the carboxylic group which results from the base-acid reaction and leads to cement formation.

Figure 8 ensures that the acid-base reaction had already been carried out between the powder of the glass and the resin materials. The decreasing band intensity of the GIC matrix is considered due to the decomposition of crystalline phases by the acid. The attack by hydrogen ions involves exchange by the modifying cations (Sr^{2+}) and rupture of the aluminum network at the Al site to yield more Al ions in the cement. The release of Al cations, Sr, and fluoride is an important feature that is required for the formation of GIC.
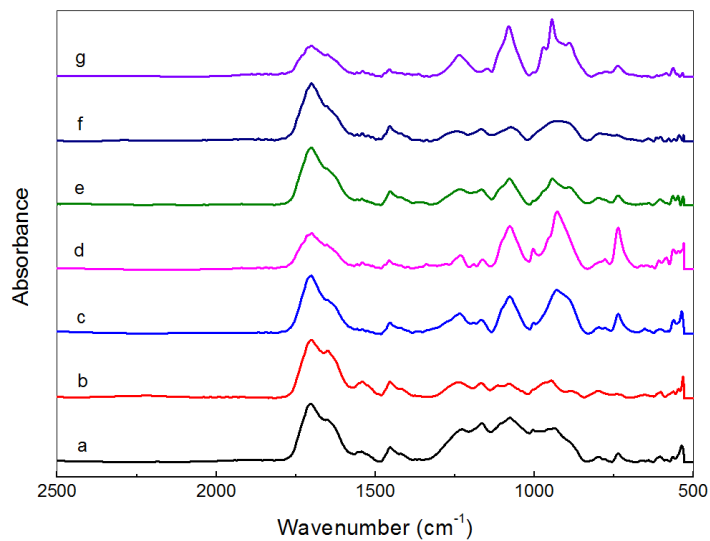
Figure 7. FTIR spectra of GIC from H.T. Al_2O_3-strontium phosphate glasses.

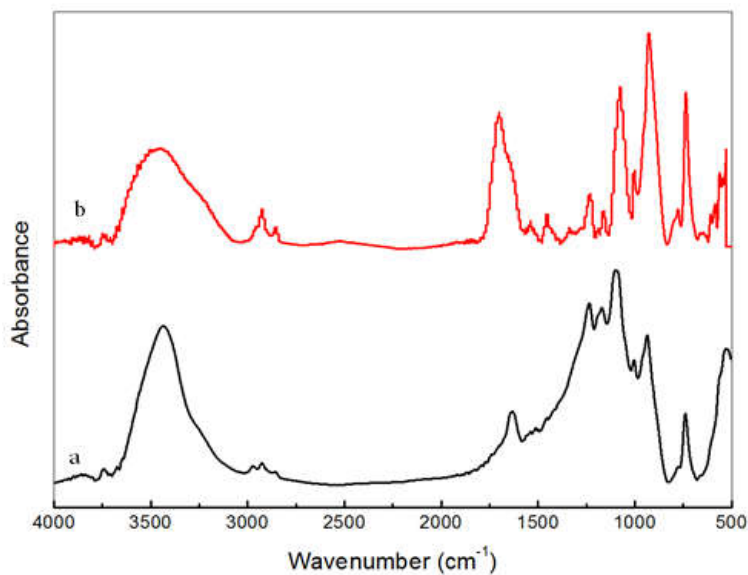
Figure 8. FTIR spectra of (a) glass sample and (b) GIC after H.T. containing 3 mol% Al_2O_3.

There is a layer containing a mixture of organic and inorganic species is formed. The well-formed layer has criteria for its resistance to acid and base treatment. Moreover, it contains crystalline apatite species which would be considered the main requirement of material compatibility and bioactivity.

CONCLUSIONS

A series of strontium-phosphate glasses with varying Al_2O_3 concentrations is successfully prepared using the melt annealing technique. The X-ray diffraction measurement has shown that there is no crystalline structure to be observed. Thermal heat treatment leads to the formation of crystalline species, which simulate dental application. The FTIR spectral experimental data of Al_2O_3-strontium phosphate glasses have shown that there is a carboxyl group that ensures cement formation. Depending on NMR and XRD results, the sample containing 3 mol% Al_2O_3 can be considered the recommended sample for GIC dental applications.

REFERENCES

1. Abdelghany, A.M.; El-Damrawi, G.; Oraby, A.H.; Madshal, M.A. Optical and FTIR structural studies on CoO-doped strontium phosphate glasses. *J. Non. Cryst. Solids*. **2018**, 499, 153-158.
2. Han, L.; Song, J.; Zhang, Q.; Luo, Z.; Lu, A. Crystallization, structure and characterization of $MgO-Al_2O_3-SiO_2-P_2O_5$ transparent glass-ceramics with high crystallinity. *J. Non. Cryst. Solids* **2018**, 481, 123-131.
3. Brow, R.K. The structure of simple phosphate glasses. *J. Non. Cryst. Solids* **2000**, 263, 1-28.
4. Bergo, P.; Reis, S.T.; Pontuschka, W.M.; Prison, J.M.; Motta, C.C. Dielectric properties and structural features of barium-iron phosphate glasses. *J. Non. Cryst. Solids*. **2004**, 336, 159-164.
5. Sene, F.F.; Martinelli, J.R.; Gomes, L. Optical and structural characterization of rare earth doped niobium phosphate glasses. *J. Non. Cryst. Solids* **2004**, 348, 63-71.
6. Kumar, S.; Vinatier, P.; Levasseur, A.; Rao, K.J. Investigations of structure and transport in lithium and silver borophosphate glasses. *J. Solid State Chem.* **2004**, 177, 1723-1737.
7. Wei, T.Y.; Hu, Y.; Hwa, L.G. Structure and elastic properties of low-temperature sealing phosphate glasses. *J. Non. Cryst. Solids* **2001**, 288, 140-147.
8. Abdelghany, A. M.; Kamal, H. Spectroscopic investigation of synergetic bioactivity behavior of some ternary borate glasses containing fluoride anions. *Ceram. Int.* **2014**, 40, 8003-8011.
9. Sene, F.F.; Martinelli, J.R.; Okuno, E. Synthesis and characterization of phosphate glass microspheres for radiotherapy applications. *J. Non. Cryst. Solids* **2008**, 354, 4887-4893.
10. Elbashar, Y.H.; Ali, M.I.; Shaikh, H.A.; Mostafa, A.G. E. D. Influence of CuO and Al_2O_3 addition on the optical properties of sodium zinc phosphate glass absorption filters. *Optik* **2016**, 127, 7041-7053.
11. Ibrahim, A.M.; Elbashar, Y.H.; Badr, A.M.; Elshaikh, H.A.; Mostafa, A.G. Mixed ionic–polaronic conduction in copper sodium phosphate glasses containing aluminium oxide. *J. Microw. Power Electromagn. Energy* **2017**, 51, 71-89.
12. Koudelka, L.; Mošner, P.; Zeyer, M.; Jäger, C. Lead borophosphate glasses doped with titanium dioxide. *J. Non. Cryst. Solids* **2003**, 326, 72-76.
13. Okada, G.;Shinozaki, K.; Komatsu, T.; Kawano, N.; Kawaguchi, N.; Yanagida, T. Tb^{3+}-doped $BaF_2-Al_2O_3-B_2O_3$ glass and glass-ceramic for radiation measurements. *J. Non. Cryst. Solids* **2018**, 501, 111-115.
14. Tarafder, A.; Molla, A.R.; Mukhopadhyay, S.; Karmakar, B. Fabrication and enhanced photoluminescence properties of Sm^{3+}-doped $ZnO–Al_2O_3–B_2O_3–SiO_2$ glass derived willemite glass–ceramic nanocomposites. *Opt. Mater.* **2014**, 36, 1463-1470.
15. Fabris, D.C.N.; Polla, M.B.; Acordi, J.; Luza, A.L.; Bernardin, A.M.; De Noni Jr, A.; Montedo, O.R.K. Effect of $MgO \cdot Al_2O_3 \cdot SiO_2$ glass-ceramic as sintering aid on properties of alumina armors. *Mater. Sci. Eng. A* **2020**, 781, 139237.

16. Abdelghany, A.M.; Rammah, Y.S. Transparent alumino lithium borate glass-ceramics: Synthesis, structure and gamma-ray shielding attitude. *J. Inorg. Organomet. Polym. Mater.* **2021**, 31, 2560-2568.

17. Pershina, S.V.; Il'ina, E.A.; Druzhinin, K.V.; Farlenkov, A.S. Effect of $Li_2O–Al_2O_3–GeO_2–P_2O_5$ glass crystallization on stability versus molten lithium. *J. Non. Cryst. Solids*. **2020**, 527, 119708.

18. Hou, Y.; Cheng, J.; Kang, J.; Yuan, J.; Cui, J. Structure, glass stability and rheological properties of $Na_2O–CaO–Al_2O_3–SiO_2$ glasses doped with Y_2O_3. *Ceram.-Silik.* **2018**, 62, 173-180.

19. Souissi, F.Z.; Ettoumi, H.; Barré, M.; Toumi, M. Preparation and electrical conductivity of potassium phosphate glasses containing Al_2O_3. *J. Non. Cryst. Solids* **2018**, 481, 585-589.

20. El-Damrawi, G.; Hassan, A.K.; Shahboub, A. Characteristic studies on $Ag_2O-Al_2O_3-P_2O_5$ glasses and glass ceramics. *J. Mater. Sci. Eng., B* **2021**, 264, 114957.

21. Kato, K.; Hayakawa, T.; Kasuya, Y.; Thomas, P. Influence of Al_2O_3 incorporation on the third-order nonlinear optical properties of $Ag_2O–TeO_2$ glasses. *J. Non. Cryst. Solids* **2016**, 431, 97-102.

22. Ramzi, Z.; Touhtouhou, S.; Taibi, M.H.; Bettach, M.; Hajjaji, A.; Nachit, W.; Benkhouja, K. Synthesis and characterization of new amorphous phases in $Bi_2O_3-P_2O_5-SrO$ system. *Int. J. Eng. Adv. Technol.* **2014**, 4, 55-57.

23. Eckert, H. Structural characterization of bioactive glasses by solid state NMR. *J. Solgel Sci. Technol.* **2018**, 88, 263-295.

24. El -Damrawi, G.; Abdelghany, M.; Mnaaa, E. Nuclear magnetic resonance studies on vanadium phosphate glasses. *Magn. Reson. Solids* **2019**, 21, 19504.

25. El -Damrawi, G.; Salaheldin, H.; Abdelghany, M. Structural investigations on inorganic $Al_2O_3–ZnO$ composites. *J. Appl. Phys A* **2021**, 127, 1-6

26. El-Damrawi, G.; Hassan, A.K.; Shahboub, A. [31]P and [27]Al nuclear magnetic resonance studies on silver phosphate glasses. *Magn. Reson. Solids*. **2018**, 20, 18202.

27. Bhogi, A.; Srinivas, B.; Papolu, P.; Shareefuddin, M.; Kistaiah, P. Effect of Mn^{2+} ions on spectroscopic and electrical properties of lithium strontium borate glasses. *Mater. Chem. Phys.* **2022**, 291, 126698.

28. Abdallah, E.M.; Meikhail, M.S.; El-Adawy, A.; Othman, H.A.; Abdelghany, A.M. Structural and antibacterial peculiarities of modified borate bioglass containing mixed dopant oxides. *J. Bio- Tribo-Corros.* **2022**, 8, 1-11.

29. Madshal, M.A.; Abdelghany, A.M.; Abdelghany, M.I.; El-Damrawi, G. Biocompatible borate glasses doped with Gd_2O_3 for biomedical applications. *Eur. Phys. J. Plus*. **2022**, 137, 1-14.

30. Fazal, S.; Zaman, F.; Ali, S.; Iqbal, Y.; Chanithima, N.; Tuscharoen, S.; Ali, M.; Hayat, K.; Zulfiqar, S.; Arshad, M.; El-Denglawey, A.; Kaewkhao, J. Investigation of europium-doped aluminium phosphate glass for red light generation. *Ceram. Int.* **2022**, 48, 24751-24757.

31. Fuchs, M.; Gentleman, E.; Shahid, S.; Hill, R.G.; Brauer, D.S. Therapeutic ion-releasing bioactive glass ionomer cements with improved mechanical strength and radiopacity. *Front. Mater.* **2015**, 2, 63.

32. Alhalawani, A.M.; Mehrvar, C.; Stone, W.; Waldman, S.D.; Towler, M.R. A novel tantalum-containing bioglass. Part II. Development of a bioadhesive for sternal fixation and repair. *Mater. Sci. Eng. C* **2017**, 71, 401-411.